Generation of Micromonodispersed Droplets and Bubbles in the Capillary Embedded T-Junction Microfluidic Devices

K. Wang, Y. C. Lu, J. H. Xu, J. Tan, and G. S. Luo
Dept. of Chemical Engineering, The State Key Lab of Chemical Engineering, Tsinghua University, Beijing 100084, China

DOI 10.1002/aic.12263
Published online April 28, 2010 in Wiley Online Library (wileyonlinelibrary.com).

This work focuses on the dispersion of micromonodispersed droplets and bubbles in the capillary embedded T-junction microfluidic devices. The effects of the microchannel structure, operating conditions, and physical properties on the dispersion rules were carefully investigated. It was found that the extended capillary could greatly affect the dispersion rules, which was favorable for reducing the dispersed size. The dispersed size was mainly dominated by the Ca number, and the effects of dispersed phase flow rate and viscosity ratio of the two phases were also very important. The dispersion mechanism and size rules in the capillary embedded microfluidic devices were discussed seriously by comparing the similarities and differences of the liquid/liquid and gas/liquid dispersion processes. © 2010 American Institute of Chemical Engineers *AIChE J,* 57: 299–306, 2011

Keywords: microfluidic, T-junction, capillary, droplet, bubble

Introduction

Multiphase flowing systems play an essential role in science and technology with various applications such as chemical engineering, environment, energy, and other processes. During recent years, microdispersed liquid/liquid and gas/liquid systems have caught the attention of many researchers for their controllable flow and effective transport properties. It has been found that the heat and mass transfer rates can be significantly increased with the reduction of dispersed size.[1–3] By using microfluidic devices, micromonodispersed bubbles and droplets can be prepared, which are more useful for research and production processes. Several methods have been developed to prepare microdroplets and microbubbles with microfluidic devices, such as cross-flowing shearing,[4] perpendicular flowing shearing,[5] hydrodynamic flow focusing,[6] coflowing rupturing,[7] and geometry-dominated breakup.[8] Among them, the cross-flowing shearing method in the T-junction microchannel is more favorable for the application in chemical engineering processes because of the simple device structure.[2,9]

The dispersion mechanism and size rules are very important for the application of microfluidic devices. Thorsen et al. first investigated the preparation of microdroplets in a T-junction microchannel.[10] They described the droplet size was mainly determined by the forces balance of interfacial tension and viscous shearing force. In the following studies, several novel phenomena in the dispersion process were discovered. Three regimes of the rupturing process "squeezing, dripping, and jetting" have been found and the break-up mechanisms have been seriously investigated.[11–13] The capillary number (Ca) is a character parameter in dispersion process. At Ca value lower than 0.01, it is generally realized that the break-up of droplets is mainly dominated by the squeezing pressure and plug-like droplets are prepared in this situation. At Ca number higher than 0.01, round droplets are more likely dripping off in the T-junction devices which is dominated by viscous shearing force and interfacial tension. Besides those forces, recent study has shown that the squeezing pressure cannot be neglected in the dripping

Correspondence concerning this article should be addressed to G. S. Luo at gsluo@tsinghua.edu.cn.

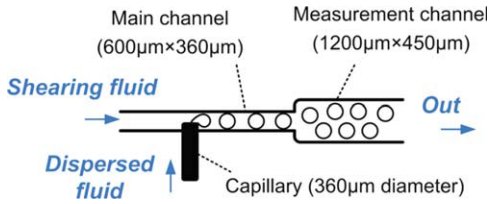

Figure 1. The sketch view of capillary embedded T-junction microfluidic device.

The sizes of the channels are shown as width × height in the figure and the flow directions are indicated by the arrows. [Color figure can be viewed in the online issue, which is available at wileyonlinelibrary.com.]

regime either.[12] The formation of jetting dispersion is more complicated. High Ca number, high viscosity, and phase ratio of dispersed phase to continuous phase can cause downstream movement of the detachment point from the channel junction, which induces jetting-mode rupture.[14] The dispersed sizes of the droplets and bubbles are mainly determined by the volume phase ratio of the two phases in the squeezing regime.[13] While in the dripping regime, the droplet sizes are mainly determined by the Ca number, phase ratio, and viscosity ratio.[11,12]

In the previous studies of T-junction microfluidic devices, almost all the channel junctions are rigidly T-shaped, and the investigations usually focus on the operating conditions and the physical properties such as phase ratio, shearing force,[15] interfacial tension,[16] and viscosity.[14] However, the effect of the channel structure on the dispersion process has not been discussed enough. In our previous works, we made some researches in this field. The liquid/liquid dispersion process in a double-pore T-junction microfluidic device was investigated and it was found that there was an extrusion effect between the growing droplets.[17] The gas/liquid dispersion process in a series of T-junction microchannels with various inject angles of the liquid phase was investigated too and it was found that the predicted equation of the gas plug length should be modified with the intersecting angle of channel junctions.[18]

In this work, we try to give a further investigation on the dispersion process of the capillary embedded T-junction microchannel, which was developed in our lab before.[19,20] The tip of the capillary is extended into the main channel, and the geometric structure is changed with the variation of capillary extended length. The dispersion rules for liquid/liquid and gas/liquid systems in the dripping regimes are investigated and some dispersion phenomena are discussed in detail too. With the comparison of liquid/liquid and gas/liquid dispersion processes, the effect of Ca number, dispersed phase flow rate, and viscosity ratio are carefully studied and the enhancement effect of the shearing force direction is also discussed with a micron-resolution particle image velocimetry (micro-PIV) system.

Experimental

The capillary embedded T-junction microfluidic devices were fabricated on polymethyl methacrylate (PMMA) chips using end mills. The main channel was 600 μm in width and 360 μm in height. A measurement channel with 1200 μm in width and 450 μm in height was fabricated directly downstream the main channel. A metal capillary with inner diameter of 190 μm and outer diameter of 370 μm was embedded into the side channel as the inlet of the dispersed phase fluids. The PMMA microchannel chip was sealed with supersonic assisted sealing technology.[21] A sketch view of the capillary embedded T-junction microfluidic device is shown in Figure 1. With the extension of the capillary into the main channel, the structure of T-junction was varied. Three kinds of microchannels labeled with T1, T2, and T3 were fabricated in this work. The extended lengths of the three kinds of microdevices are 0 μm, 290 μm, and 420 μm, respectively.

The dispersion processes of the droplets and bubbles are discussed in this work. Deionized water was used as the dispersed phase for the liquid/liquid (L/L) dispersion investigation and air was used as the dispersed phase for the gas/liquid (G/L) dispersion investigation. Three kinds of oil with surfactants were used as continuous phases. The oils have different viscosities and different interfacial tensions with water and air. The physical properties of the working systems at 20°C are given in Table 1. The viscosities were measured with an Ubbelohde viscometer. The interfacial tensions and the contact angles were measured with a pendent drop interfacial tension meter (OCAH200, DataPhysics Instruments GmbH, Germany). The contact angles were calculated with ellipse fitting method. From the contact angle data in the table, it can be seen that the continuous phases have good wetting properties with the capillary and the channel wall. For the experimental materials, the dodecane and Span85 were provided by the Sinopharm Chemical Reagent Co., Ltd (China). The mineral oil and Span80 were provided by the Beijing Modern Eastern Finechemical Co., Ltd (China).

In the experiment, all the fluids were delivered by syringe pumps (TS2-60, Longer, China) with gastight syringes. The flow pattern was controlled in the dripping regime in this work. For the comparison of the L/L and G/L dispersion process, both the feed flow rates of water and gas were controlled from 30 μl/min to 80 μl/min. Considering the wetting effect of surfactants on the channel walls, the continuous phases were pumped into the devices 30 min before the incoming of dispersed phases. After changing any of the

Table 1. Physical Properties of the Working Systems (20°C)

Oil	$C_{12}H_{26}$ + Mineral Oil	Mineral Oil	Corn Oil
Surfactant	2 wt % Span80	2 wt % Span85	2 wt % Span85
μ_C (m Pas)	4.62	24.8	72.7
γ_{WO} (mN/m)	3.79	8.10	11.5
γ_{GO} (mN/m)	21.8	22.4	31.5
α_{WMO}	155°	164°	170°
α_{GMO}	153°	158°	157°
α_{WPO}	153°	159°	163°
α_{WPO}	152°	153°	157°

The mass percentage of $C_{12}H_{26}$ in the mixing oil is 47 wt %. μ_C is the viscosity of the oil solutions, γ_{WO} is the interfacial tension of water with oil, γ_{OG} is the surface tension of air with oil, α_{WMO} is the contact angle of water on capillary metal with oil as surrounding solution, α_{GMO} is the contact angle of air on capillary metal with oil as surrounding solution, α_{WPO} is the contact angle of water on PMMA with oil as surrounding solution, and α_{GPO} is the contact angle of air on PMMA with oil as surrounding solution.

operating conditions, it was allowed at least 1 min of equilibration time. Experiments were carried out with a microscope that had a high-speed CCD video camera (PL-A742, PixeLINK, Canada). The images were recorded with a frequency of 100 images per second. The round droplets and bubbles flowing in the measurement channel were recorded and their apparent average diameter (d_{av}) were determined by measuring at least 50 droplets or bubbles. The real hydraulic diameter (d) of the droplets and bubbles were calculated by the apparent average diameter and the channel height as shown in Eq. 1.

$$d = \begin{cases} d_{av} & (d_{av} < H) \\ (6V/\pi)^{1/3} = (d_{av}^2 \cdot H)^{1/3} & (d_{av} > H) \end{cases} \quad (1)$$

where V is the volume of the droplet or bubble and H is the height of the measuring channel. The shape of the droplet was assumed as ellipsoid for the situation of $d_{av} > H$. The polydispersity index (σ) of the droplets and bubbles was also calculated, which is defined by Eq. 2,

$$\sigma = \delta/d_{av} \times 100\% \quad (2)$$

where δ is the standard deviation of the apparent droplet diameter. All the polydispersity indices at different experimental conditions were less than 3% in this work. In the experiment, the velocity fields around the growing droplets were also measured with a micro-PIV system (Dantech Dynamics, Denmark) to give a deep investigation of dispersion rules in the capillary embedded T-junction microfluidic device.

Results and Discussion

Dispersion rules at the capillary extended length = 0

To get a clear understanding of the dispersion rules in the capillary embedded T-junction microfluidic device, the dispersed sizes of the droplets and bubbles with the variation of Ca number are investigated first without extended length. The identification of Ca is

$$\mathrm{Ca} = \frac{\mu_C u_C}{\gamma} = \frac{\mu_C Q_C}{w_C h \cdot \gamma} \quad (3)$$

where μ_C is the viscosity of the continuous phase; u_C is average velocity of the continuous phase; w_C is the width of the channel junction ($w_C = 600$ μm for T1); h is the height of the channel ($h = 360$ μm); and γ is the interfacial tension. Without the extended capillary, the microfluidic device becomes a common T-junction microfluidic device with a round dispersed phase inlet. As the Ca number is high in our experiment and round droplets (bubbles) are formed in the main channels, the dispersed sizes are mainly determined by the Ca number, the same as the previous studies.[11,12] Figure 2 gives the dispersed sizes with the variation of Ca number. It can be seen that the dispersed sizes decrease with the increase of Ca dimension. However, the smallest droplets are still bigger than 200 μm, 1/3 time of the main channel width, even at the Ca > 0.3.

From the figures we can see some other information. For the L/L dispersion process, the flow rate of dispersed phase also affects the droplet size. The effect of the dispersed

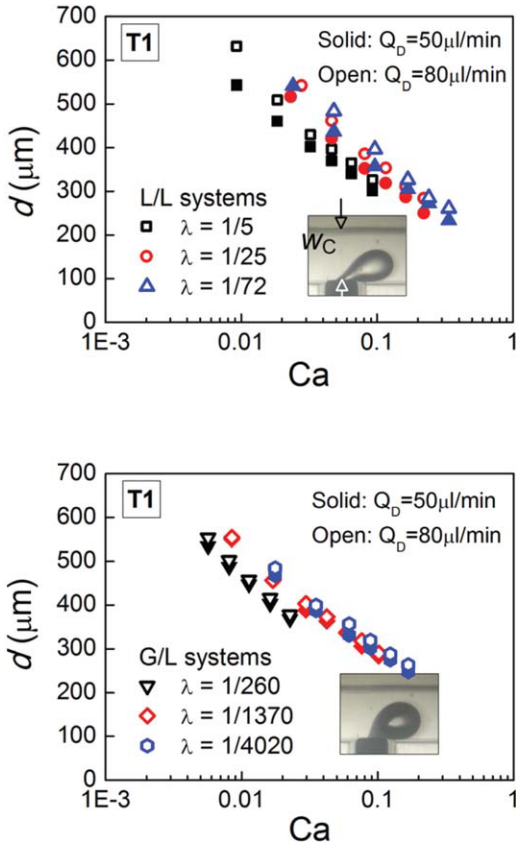

Figure 2. The dispersed sizes of the droplets and bubbles in capillary embedded T-junction microfluidic device with extended length = 0.

Q_D refers to the flow rate of dispersed phase; λ refers to the viscosity ratio ($\lambda = \mu_D/\mu_C$) [Color figure can be viewed in the online issue, which is available at wileyonlinelibrary.com.]

phase is strong at low Ca number, but becomes weak at high Ca number. The appearance of this phenomenon is due to the different phase ratios of the two processes at different dispersed phase flow rates for the same Ca number and the same working system. These results accord with the simulation of De Menech et al.[12] and their results have shown that the effect of phase ratio becomes weak with the increase of Ca value. In our experiment, the phase ratio also becomes very low at high Ca number, as we fixed the flow rate of the dispersed phase to several tens of microliters per min and changed the flow rates of continuous phase from 100 μl/min to 1400 μl/min. Thus, the effect of dispersed phase flow rate is weak at high Ca number.

While for the G/L dispersion process, the effect of the dispersed phase flow rate is not as significant as the L/L dispersion process. The reason for this phenomenon may be explained from the different growing routes of the droplet and bubble. Figure 3 shows the width (y^*) variation of droplet and bubble with time. This width variation reflects the growth of bubble and droplet. It can be seen that the growing routes for the droplets and bubbles are very different. For the L/L dispersion process, the droplet grows continuously, whereas for the G/L dispersion process, the bubble does not grow in the initial time. The appearance for this

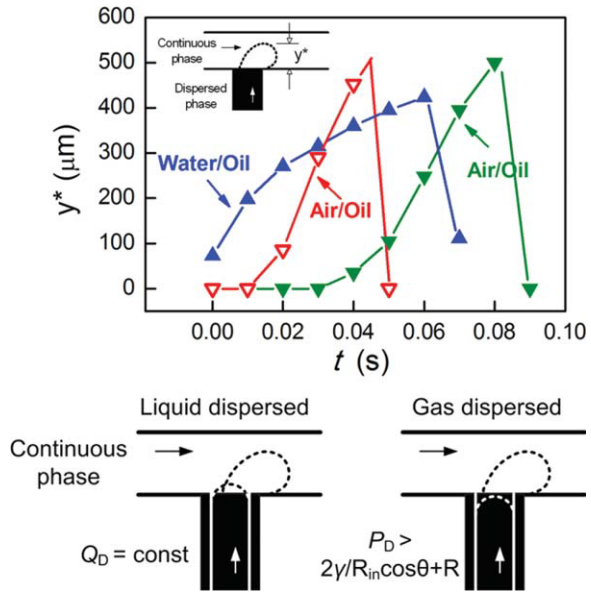

Figure 3. The variation of the droplet and bubble widths with time in the generation process.

For the L/L dispersion process: $Q_D = 50$ μl/min, $Q_C = 200$ μl/min. For the G/L dispersion process: $Q_D = 50$ μl/min (filled symbols), $Q_D = 80$ μl/min (open symbols), $Q_C = 350$ μl/min. The continuous phase is $C_{12}H_{26}$ + mineral oil with 2 wt % Span80. [Color figure can be viewed in the online issue, which is available at wileyonlinelibrary.com.]

difference is owing to the compressibility of gas phase. Water is incompressible, so the growing rate of the droplet is equal to the incoming flow rate of water. However, the incoming flow rate of air that we controlled does not represent the growing rate of the bubble. The effect of the gas flow is to increase the pressure in the capillary, and when the inner pressure of gas phase (P_D) becomes higher than the sum of Laplace pressure ($2\gamma/R_{in}\cos\theta$, R_{in} is the inner radius of the capillary and θ is the contact angle) and flowing resistance (R), the bubble begins to grow. As the bubble grows the Laplace pressure decreases, so the bubble size enlarges quickly with the release of pressure. From this mechanism, it can be seen that increasing the gas flow rate just increase the pressure growing speed, but it has weak effect on the growing and rupturing processes. Hence the effect of dispersed phase flow rate is weak on the G/L dispersion process.

From Figure 2, we can also see the effect of viscosity ratio ($\lambda=\mu_D/\mu_C$) on the dispersion process. Three kinds of oils with viscosities ranging from 4.6 to 73 were used in this work. For the L/L dispersion process, high viscosity ratio causes small droplets. According to the researches of Anna and coworkers,[11] the droplet size does not change with the viscosity ratio when it is lower than 1/50. In this work, we changed the viscosity ratio just beside this critical value. Thus, the droplet size changes all the time. While for the G/L dispersion process, it is found that the dispersed sizes are not changed at the viscosity ratios of 1/1370 and 1/4020. The reason for the variation of the droplet size with the change of the viscosity ratio is not clear now. But what we found from the recoded pictures at the rupturing moment may be useful to explain this. We measured the width (y^*) and the mid-line length (l^*) of the droplet and bubble at the moment before they accelerate to rupture off, and it is found that the ratios of y^* to l^* are changed with the changing of viscosity ratio, as shown in Figure 4. High viscosity ratio causes strong elastic deformation and low height–length ratio droplets are formed at the channel junction (bubbles), which affects the volume of the dispersed phase. For the same Ca number of the continuous phases, it is found that the height of the rupturing droplet changes little due to the force balance of the shearing stress, squeezing pressure, and interfacial tension. Thus, long rupturing droplets causes large volume and big size of the dispersed droplets at low viscosity ratio.

Dispersion rules at the capillary extended length > 0

For the chemical engineering process, small-scale droplets or bubbles are needed sometimes to get highly efficient mass and heat transport properties of the working systems. According to the above analysis, using viscous continuous phase is helpful to obtain small dispersed sizes. However, sometimes we are not allowed to change the working system either. Thus, new method should be invited to solve this problem. Lee et al. developed a moving wall T-junction microfluidic device to increase the sharing speed at the channel junction.[15] Their method is effective, but it is only useful in the devices fabricated with soft materials. While for the chemical engineering process, most devices are fabricated with hard materials. By using capillary embedded devices, the enhancement of sharing velocity can be solved with an extended capillary tip.

Figure 5 shows the dispersion processes in the three kinds of microchannels in the same range of continuous phase

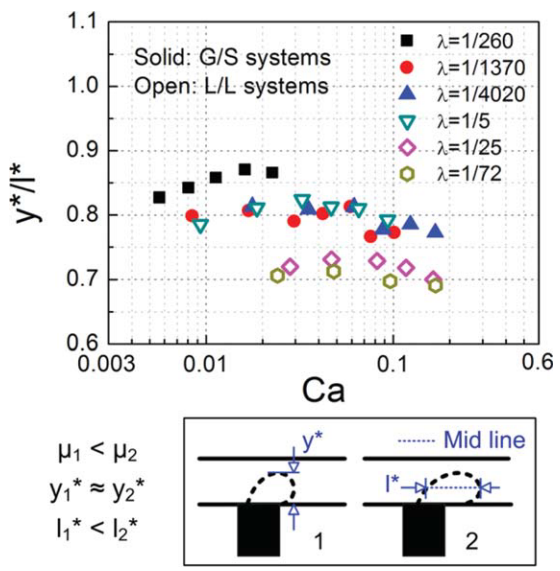

Figure 4. The height–length ratio of the rupturing droplets and bubbles.

$Q_D = 50$ μl/min in the figure [Color figure can be viewed in the online issue, which is available at wileyonlinelibrary.com.]

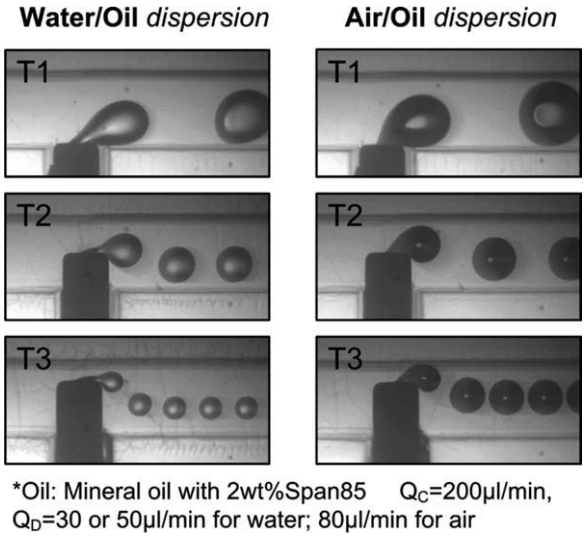

Figure 5. The micrographs of the channel junctions used for L/L and G/L dispersion processes.

The metal capillaries are black in the micrographs.

flow rate. It can be seen that the dispersed sizes decrease obviously with the extension of capillary tip into the main channel. The sharing speed is enhanced with the narrowing of the channel. As the shearing effect only acts on the rupturing position, we just need to adjust the structure at the channel junction to enhance the shearing effect. In this work, the main channels were narrowed to 1/2 and 1/3 time from the original channel in devices T2 and T3, thus the shearing speed can be increased two and three times. Figure 6 gives an example of the droplet and bubble sizes in three kinds of microfluidic devices with $C_{12}H_{26}$ + mineral oil as oil. With the extended capillaries, the consumption of continuous phase can be reduced for the generation of small droplets and bubbles.

To give a clear description of the dispersion rules as Figure 2 given, we plot the dispersed sizes of different working systems with the variation of Ca numbers in the microfluidic devices T2 and T3, as shown in Figure 7. As the average shearing velocity is the flow speed on the capillary tip, the width of the channel junction was considered as the width of the slot to calculate the Ca number (w_C = 310 μm for T2 and 180 μm for T3). From Figure 7, it can be seen that the effects of Ca number, dispersed phase flow rate, and viscosity ratio on the dispersed sizes in the extended capillary devices are the same as the common T-junction devices. The smallest droplet and bubble sizes are about 100 μm and the Ca number can reach to 0.6.

Comparing with the dispersed sizes of bubbles and droplets in different microchannels, we found some more interesting results. It is found that the channel structure affects the dispersed size too. For the same Ca value and the same working system, the dispersed sizes are small with long extended length. Figure 8 gives a comparison of the droplet and bubble sizes in the three kinds of microchannels. Both the L/L and G/L dispersion processes exhibit this phenomenon. To give a deep understanding of the dispersion process at the channel junctions, we measured the velocity fields around the growing droplet using a micro-PIV system. Figure 9 gives some examples of the rupturing moment in T1, T2, and T3. The velocity fields are clearly displayed in the figure and it can be seen the continuous phase passes through the growing droplet and moves forward the channel in the common T-junction device. This shearing fluid gives an average shearing force on the droplet paralleling the main channel. While in the capillary extended T-junction microchannel, the continuous phase also passes through the growing droplet but turns to the bottom side of the channel behind the droplet. This flow direction change provides a deflected average shearing force on the droplet, which enhances the shearing process at the channel junction. This deflected shearing force direction may be the reason for the size difference at different extended length. As the Ca number only provides the value ratio of the incoming shearing force and interfacial tension, which cannot reflect the force directions, the dispersed size varies at the same Ca value with the change of the force directions.

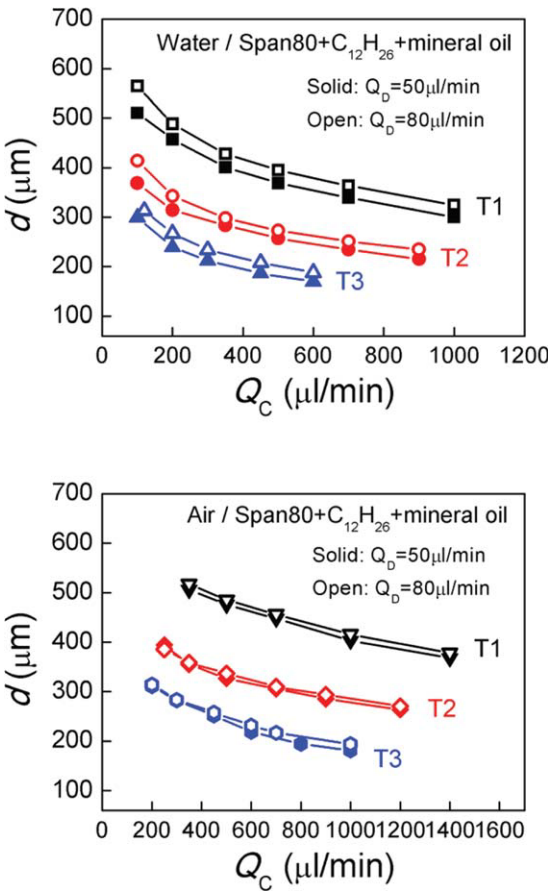

Figure 6. The dispersed sizes of droplets and bubbles in the microfluidic devices with $C_{12}H_{26}$ + mineral oil (2 wt % Span85) as oil phase.

[Color figure can be viewed in the online issue, which is available at wileyonlinelibrary.com.]

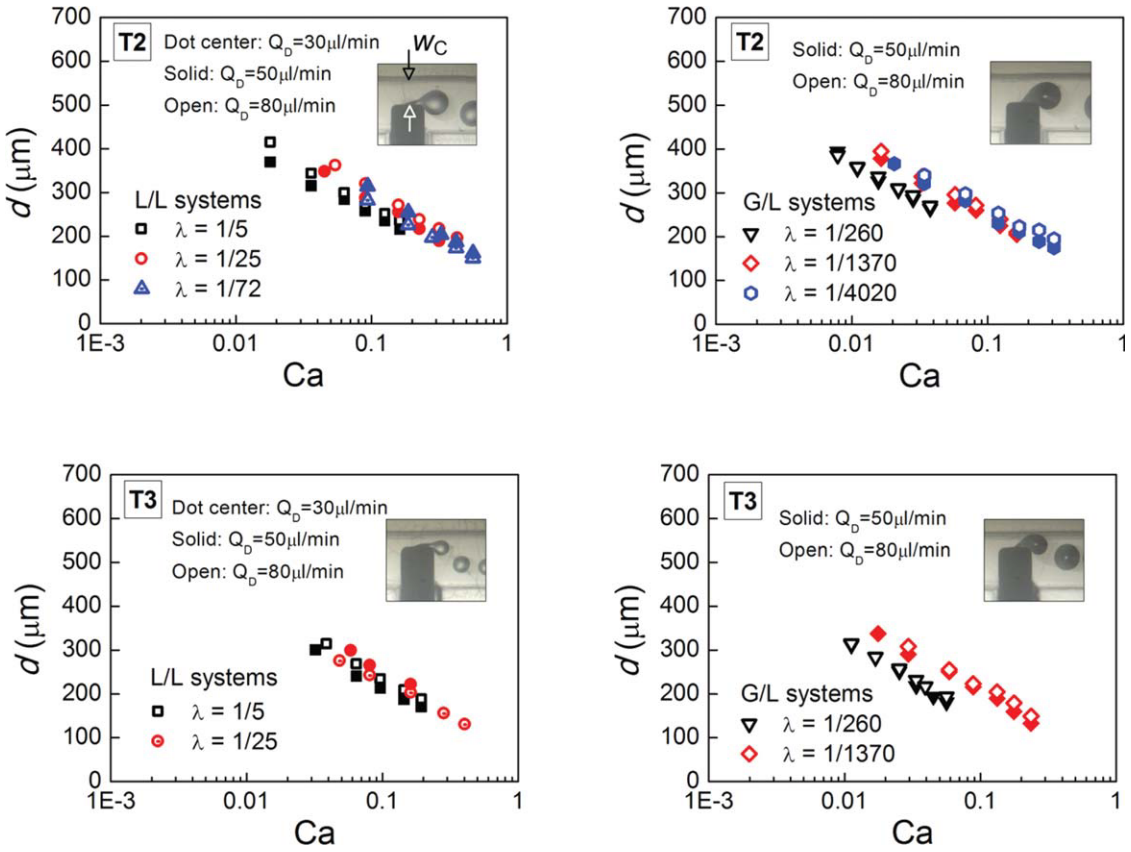

Figure 7. The dispersed sizes of the droplets and bubbles in capillary embedded T-junction microfluidic device with extended length > 0.

[Color figure can be viewed in the online issue, which is available at wileyonlinelibrary.com.]

Similarity of L/L and G/L size rules

In the above analysis, we show the differences between L/L and G/L dispersion process, such as the effects of dispersed phase flow rate, viscosity ratio, and droplet growing routes. While, as cross-shearing break-up processes they have similarities too. Both the droplet and bubble rupture when the force balance is achieved, and the Ca number is an important criterion for the dispersed size. In the previous studies, complicated mathematical models and simple power-law relations with Ca number have been used to predict the dispersed sizes in the T-junction microfluidic devices.[11,22] To give a clear explanation about the similarity of the size rules in L/L and G/L dispersion process, we correlated the dispersed sizes in our experiment with power-law relations and it is found that the indexes of Ca number exist in the similar range for the L/L and G/L dispersion processes. We

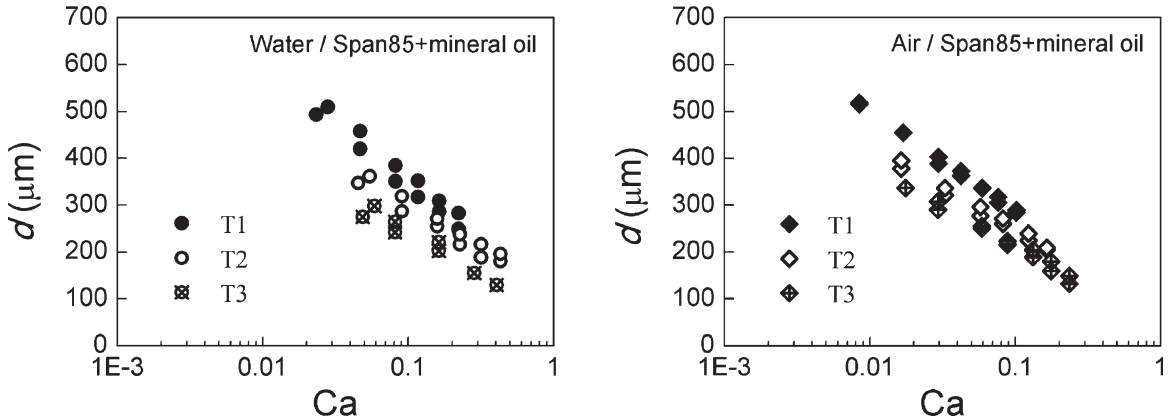

Figure 8. Effect of channel structure on the dispersion rules in the capillary embedded T-junction microfluidic device.

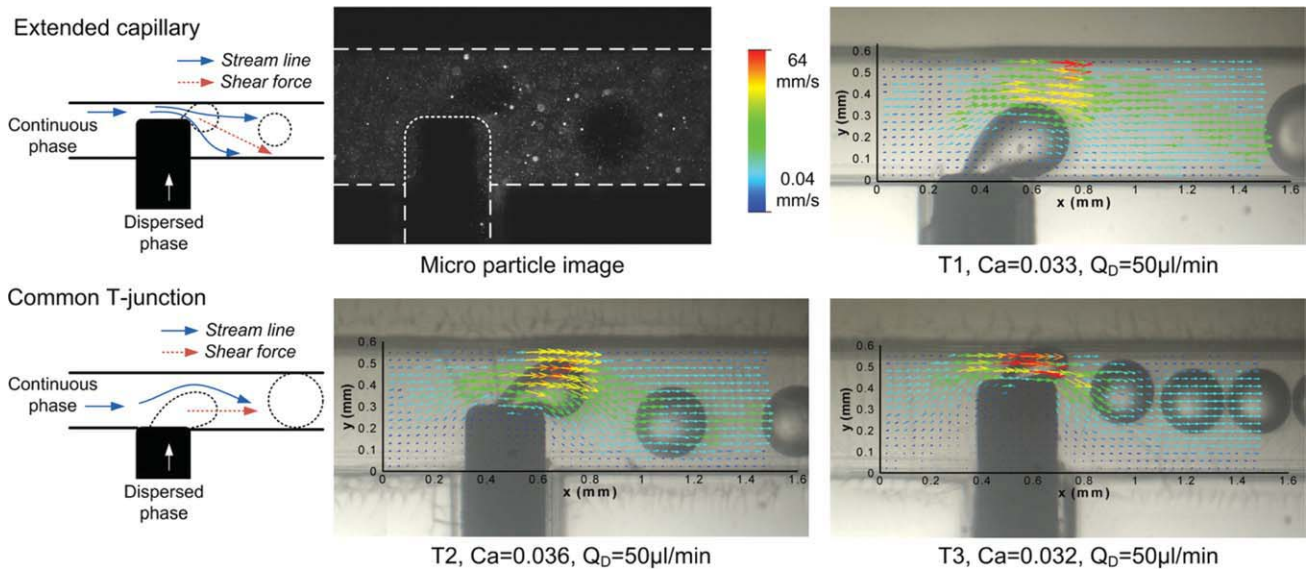

Figure 9. Micro-PIV investigation on shearing force direction with different extended capillary lengths.

[Color figure can be viewed in the online issue, which is available at wileyonlinelibrary.com.]

correlated all groups of the experimental data for each working system and each extended length, and found the index of Ca exits in a narrow range, from −0.25 to −0.34 for the L/L dispersion process and from −0.23 to −0.31 for the G/L dispersion process, as shown in Figure 10. This result accords with the previous studies of ourselves and other groups.[12,16,23] Although the physical meaning of the index has not been discussed clearly until now, it still shows the similarity of L/L and G/L dispersion processes.

Conclusion

In this work, the dispersion rules of L/L and G/L microdispersion processes in the capillary embedded T-junction microfluidic devices have been investigated. The structure of the microfluidic devices is varied with extending the capillary tip into the main channel and it is found that this structure change can greatly reduce the dispersed sizes with low consumption of continuous phase fluid. The flowing characters of the L/L and G/L dispersion processes in three kinds of capillary embedded T-junction microchannels have been carefully investigated by considering the effects of capillary number, dispersed phase flow rate, and viscosity ratio of the two phases. It is found that the dispersed sizes decrease with a power-law relation with the increase of Ca value, which index ranges from −0.23 to −0.34. The effect of the dispersed flow rate is strong in the L/L dispersion process but becomes weak in the G/L dispersion process. The reason for this phenomenon can be explained from the different growing routes of the droplets and bubbles. Besides it is found that low viscosity ratio of dispersed phase to continuous phase provides large dispersed size due to the elastic deformation of the dispersed phases. Additionally, it is found that the direction of shearing force is very important for the dispersion process too.

Furthermore, those T-junction microfluidic device with an embedded capillary can be applied into many areas, as monodispersed microdroplets smaller than the channel scale

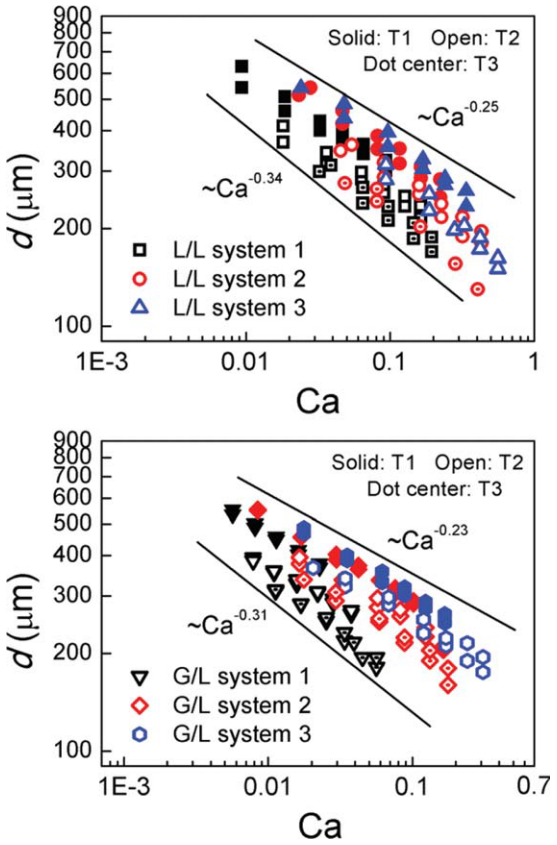

Figure 10. The similar power-law relations of L/L and G/L dispersion process in the capillary embedded T-junction microfluidic devices.

The slopes of the black lines refer to the maxim and minim of the indexes of Ca. System 1 refers to $C_{12}H_{26}$ + mineral oil with Span80 as the continuous phase; System 2 refers to mineral oil with Span85 as the continuous phase; System 3 refers to corn oil with Span85 as the continuous phase. [Color figure can be viewed in the online issue, which is available at wileyonlinelibrary.com.]

can be easily prepared with low cost of the continuous phase, which is benefit for many application process, such as the preparation of microbead and microspheres. In this work, the capillary was fixed in the side channel for the consideration of sealing. If the capillary is designed as a sliding structure with modified fabrication technique, the size of the droplet can be changed optionally by verifying the extended length of the capillary without changing flow rates.

Acknowledgments

We would like to acknowledge the support of the National Natural Science Foundation of China (20525622, 20876084, and 20806042) and the National Basic Research Program of China (2007CB714302) for this work.

Literature Cited

1. Cristini V, Tan YC. Theory and numerical simulation of droplet dynamics in complex flows—a review. *Lab Chip*. 2004;4:257–264.
2. Dessimoz AL, Cavin L, Renken A, Kiwi-Minsker L. Liquid-liquid two-phase flow patterns and mass transfer characteristics in rectangular glass microreactors. *Chem Eng Sci*. 2008;63:4035–4044.
3. Wang K, Lu YC, Shao HW, Luo GS. Heat-transfer performance of a liquid-liquid microdispersed system. *Ind Eng Chem Res*. 2008; 47:9754–9758.
4. Xu JH, Li SW, Tan J, Luo GS. Correlations of droplet formation in T-junction microfluidic devices: from squeezing to dripping. *Microfluid Nanofluid*. 2008;5:711–717.
5. Tan J, Xu JH, Li SW, Luo GS. Drop dispenser in a cross-junction microfluidic device: scaling and mechanism of break-up. *Chem Eng J*. 2008;136:306–311.
6. Nie ZH, Seo MS, Xu SQ, Lewis PC, Mok M, Kumacheva E, Whitesides GM, Garstecki P, Stone HA. Emulsification in a microfluidic flow-focusing device: effect of the viscosities of the liquids. *Microfluid Nanofluid*. 2008;5:585–594.
7. Utada AS, Fernandez-Nieves A, Stone HA, Weitz DA. Dripping to jetting transitions in coflowing liquid streams. *Phys Rev Lett*. 2007; 99:094502.
8. Link DR, Anna SL, Weitz DA, Stone HA. Geometrically mediated breakup of drops in microfluidic devices. *Phys Rev Lett*. 2004;92: 054503.
9. Jönsson C, Lundgren S, Haswellb SJ, Moberg C. Asymmetric catalysis in a micro reactor-Ce, Yb and Lu catalysed enantioselective addition of trimethylsilyl cyanide to benzaldehyde. *Tetrahedron*. 2004;60:10515–10520.
10. Thorsen T, Roberts RW, Arnold FH, Quake SR. Dynamic pattern formation in a vesicle-generating microfluidic device. *Phys Rev Lett*. 2001;86:4163–4166.
11. Christopher GF, Noharuddin NN, Taylor JA, Anna SL. Experimental observations of the squeezing-to-dripping transition in T-shaped microfluidic junctions. *Phys Rev E*. 2008;78:036317.
12. De Menech M, Garstecki P, Jousse F, Stone HA. Transition from squeezing to dripping in a microfluidic T-shaped junction. *J Fluid Mech*. 2008;595:141–161.
13. Garstecki P, Fuerstman MJ, Stone HA, Whitesides GM. Formation of droplets and bubbles in a microfluidic T-junction—scaling and mechanism of break-up. *Lab Chip*. 2006;6:437–446.
14. Tice JD, Lyon AD, Ismagilov RF. Effects of viscosity on droplet formation and mixing in microfluidic channels. *Anal Chim Acta*. 2004;507:73–77.
15. Lin YH, Lee CH, Lee GB. Droplet formation utilizing controllable moving-wall structures for double-emulsion applications. *J Microelectromech Syst*. 2008;17:573–581.
16. Wang K, Lu YC, Xu JH, Luo GS. Determination of dynamic interfacial tension and its effect on droplet formation in the T-shaped microdispersion process. *Langmuir*. 2009;25:2153–2158.
17. Wang K, Lu YC, Xu JH, Tan J, Luo GS. Liquid-liquid micro-dispersion in a double-pore T-shaped microfluidic device. *Microfluid Nanofluid*. 2009;6:557–564.
18. Tan J, Li SW, Wang K, Luo GS. Gas-liquid flow in T-junction microfluidic devices with a new perpendicular rupturing flow route. *Chem Eng J*. 2009;146:428–433.
19. Xu JH, Li SW, Tan J, Wang YJ, Luo GS. Preparation of highly monodisperse droplet in a T-junction microfluidic device. *AIChE J*. 2006;52:3005–3010.
20. Xu JH, Li S, Chen GG, Luo GS. Formation of monodisperse microbubbles in a microfluidic device. *AIChE J*. 2006;52:2254–2259.
21. Li SW, Xu JH, Wang YJ, Lu YC, Luo GS. Low-temperature bonding of poly-(methyl methacrylate) microfluidic devices under an ultrasonic field. *J Micromech Microeng*. 2009;19:015035.
22. Husny J, Cooper-White JJ. The effect of elasticity on drop creation in T-shaped microchannels. *J Non-Newtonian Fluid Mech*. 2006;137:121–136.
23. van der Graaf S, Nisisako T, Schroën CGPH, van der Sman RGM, Boom RM. Lattice boltzmann simulations of droplet formation in a T-shaped microchannel. *Langmuir*. 2006;22:4144–4152.

Manuscript received July 13, 2009, revision received Jan. 22, 2010, and final revision received Mar. 24, 2010.